Polymers

CrossMark

Highly stretchable fiber-shaped e-textiles for strain/pressure sensing, full-range human motions detection, health monitoring, and 2D force mapping

Song Chen[1], Shuqi Liu[1], Pingping Wang[1], Haizhou Liu[1], and Lan Liu[1,*]

[1] College of Materials Science and Engineering, Key Lab of Guangdong Province for High Property and Functional Macromolecular Materials, South China University of Technology, Guangzhou 510640, People's Republic of China

ABSTRACT

Textile-based electronics (e-textiles) have attracted huge attention in wearable sensors recently. Even though highly sensitive textile-based pressure sensors and highly stretchable textile-based strain sensors are widely researched and reported in recent years, it is still full of challenges to develop high stretchable textile-based sensors simultaneously and satisfy strain and pressure sensing, which is necessary for full-range detection of human motions. On the other hand, compared to traditional planar e-textiles, fiber-shaped e-textiles have plenty of advantages due to their fibrous architecture with lightweight, portable, skin compliant, and easily weave properties. In this work, a fiber-shaped textile, knitted with hierarchical polyurethane (PU) fibers, is used to fabricate a multifunctional e-textile by coating of silver nanowires (AgNWs) and styrene–butadiene–styrene. Due to the AgNWs conductive networks, the inherent stretchability of PU fibers, and the hierarchical structure, the as-prepared e-textile exhibits high conductivity, high stretchability, high sensitivity, and multi-detection of strain and pressure. What is more, the fabricated multifunctional e-textiles are also successfully weaved into electronic fabric for 2D force mapping. The simple, scalable strategy endows the multifunctional e-textiles great potentials in full-range detection and health care areas.

Introduction

In recent years, e-textiles, as new-fashioned wearable devices, have drawn surging attention in applications such as artificial skins, motion detection, and health monitoring systems since they can perfectly combine the functionality of wearable electronics with the soft and comfort properties of clothing [1–10]. Consequently, the developments of e-textiles with excellent responses to external stimulation are greatly desirable in this field. To date, highly sensitive textile-based pressure sensors and highly stretchable textile-

🦢 Springer

based strain sensors are widely researched for wearable devices [11–15]. Nevertheless, in addition to high sensitivity and stretchability, an ideal wearable sensor should have the ability of feeling multiple mechanical stimuli such as physical pressure and lateral strain, as it allows full-range detection of human motions (i.e., subtle vibration and large strain) just like human skin [16]. Unfortunately, almost all the above-reported e-textiles can only detect pressure or strain unilaterally; thus, it is necessary to develop humanoid e-textiles simultaneously and satisfy high stretchability, high sensitivity, and multiple sensing abilities.

From the perspective of convenient application, compared to planar and cubic wearable sensors, fiber-shaped wearable sensors have consolidated advantages of both fibers and sensors: lightweight, portable, flexible for knitting, and superb responses to mechanical deformations, which therefore make fiber-shaped wearable sensors the optimal wearable devices in the future. In this case, great efforts have been made by researchers to develop fiber-shaped sensors based on capacitive [17–19], piezoresistive [20–22], and piezoelectric effective [23, 24]. For instance, in order to make stretchable fiber-shaped strain sensors, "spring-like" [25], "wave-like" [20, 26], "knitting-based" [27], and "twining spring-like" [28] architectures were introduced into fibers for detection of tensile strain. However, as has been noted, their deficiency in sensing pressure limited their further use in detecting microphysical vibration. It is well known that special micro-/nanostructures such as "interlocked microdoms arrays" [29, 30], "silk-molded microstructures" [31], "epipremnum aureum leaves" [32], "irregular microhump structures" [33], and "hierarchical fibers" [34] were helpful to fabricate highly sensitive planar pressure sensors. Inspired by this, fiber-shaped e-textiles that integrating the above special structures will be the key to fabricate ideal wearable sensors with both fiber-shaped and strain/pressure sensing properties [35].

In this work, a fiber-shaped textile, knitted by hierarchical PU fibers, is further applied for developing e-textile by simple dip-coating of AgNWs and SBS. Because of the natural stretchability of PU fibers and the textile-based structures, the as-prepared e-textiles perform a high stretchability of 140% and a high tensile sensitivity (Gauge factor = 10.3 under strain of 2–60%, 6.3 under strain of 60–140%). In addition, the special hierarchical structure (i.e.,

hierarchical structure composed of plentiful micro-scale PU fibers) endows the e-textile a quick response to external pressure (response time of 13 ms and relax time of 53 ms) and a high pressure sensitivity $(0.20\ kPa^{-1})$. The high stretchability, high sensitivity, and multiple sensing capacities demonstrate that the as-prepared e-textiles have superb potentials in wearable devices and full-range detection of human motions. Due to the excellent flexibility and fibrous configuration, electronic fabric (e-fabric) with precise two dimensional (2D) force mapping property is also fabricated by a weaving process. Furthermore, the e-textile has a high initial conductivity, which is conducive for operation under lower voltage conditions [36]. The high-performance fiber-shaped e-textiles are promising in the applications of artificial skins, health monitoring sensors, motion sensors, smart fabrics, etc.

Materials and methods

Materials

The fiber-shaped textiles were knitted from PU fibers utilizing a Harry Lucas circular knitting machine (type R-1S). Silver nitrate ($AgNO_3$) was purchased from Beijing InnoChem Science & Technology Co., Ltd. (Beijing, China). Poly(vinylpyrrolidone) (PVP, Mw = 1300000 g/mol) was provided by J&K Technology Co., Ltd. (Beijing, China). Glycerol, ethylene glycol, anhydrous ethanol, and tetrahydrofuran (THF) were supplied by Tianjin Fuyu Fine Chemical Co., Ltd. (Tianjin, China). Sodium chloride (NaCl) was obtained from Tianjin DaMao Chemical Reagents Factory (Tianjin, China). All the chemical reagents were of analytical grade and were used as received without further purification.

Fabrication of e-textiles

AgNWs were synthesized according to our previously published works and then dispersed in anhydrous ethanol with a concentration of 3.0 mg/ml for further use [37]. After that, the knitted fiber-shaped textile was firstly dipped into the AgNWs suspension solution for 1 min and following dried at 60 °C for 10 min. (The obtained conductive textile is noted as textile-AgNWs hereafter.) The dip-coating and drying process were cycled several times for entirely

coating of AgNWs. To fix the AgNWs conductive networks, SBS was coated on the textile-AgNWs with a same dip-coating and drying method, where SBS was dissolved in THF with a mass fraction of 1 wt%. The e-textile is developed after coating of SBS. Finally, two copper wires were attached to two ends of the e-textile by conductive silver paste for resistance measurement.

Instruments

SEM and TEM images were taken using a NanoSEM 430 instrument (FEI Co. Ltd., Hillsboro, America) and a JEOL JEM-2100HR instrument (EDAX Inc., Mahwah, America), respectively. The resistance of the e-textile was measured by a TEGAM 1740 microohmmeter. The stretching and pressure test of the e-textile and recycle experiment were all carried out at room temperature using a tensile testing machine (KJ-1065A, Dongguan kejian Instruments Co., Ltd. China).

Results and discussion

Figure 1a presents a schematic illustration of the fabrication strategy of the e-textile and e-fabric. (More details can be seen in the experimental section.) Typically, a cleaned fiber-shaped textile was knitted by PU fibers (as shown in Fig. S1a, b, supporting information) and then dipped into AgNWs suspension for coating of AgNWs, after drying a stretchable and highly conductive textile with AgNWs networks (textile-AgNWs) was developed. Then, the e-textile was prepared after coating SBS on textile-AgNWs through a similar dip-coating process, after that the e-textiles was adopted for further sensing test in this work. E-fabric was also fabricated by weaving e-textiles into large area fabric. The optical photographs of the fiber-shaped textile and e-textile are shown in Fig. 1b; it can be seen that the e-textile has a good flexibility, machinability, and deformability. Figure 1c shows that after coating of AgNWs and SBS, the e-textile remains a high stretchability of 140% comparing with pristine fiber-shaped textile (as illustrated in Fig. S1c, supporting information). The developed e-fabric is presented in Fig. 1d, where mechanical sensor unit forms at each cross-contact (Fig. 1e). Figure 1f illustrates a typical morphology of the fiber-shaped textile. From the scanning electron

microscopy (SEM) image, we can see that the as-prepared textile has a typical textile-based structure knitted by plenty of hierarchical microscale PU fibers (about 20 μm in diameter as shown in Fig. 1g). The textile-based structure and hierarchical microscale PU fibers are proved to play a key role in fabricating wearable sensors with excellent strain/pressure sensing performance.

AgNWs are successfully integrated on the surface of PU fibers (Fig. 1h and S2, supporting information) through a capillary effect. Figure S3 (see supporting information) shows the SEM images of textiles AgNWs with different dip-coating cycles. With the increase in dip-coating cycles, the AgNWs networks on the surface of hierarchical PU fibers becomes thicker, simultaneously the gaps between neighboring hierarchical PU fibers are bridged by continuous AgNWs networks. In order to stabilize the conductive networks, SBS is used to immobilize AgNWs onto the surface of PU fibers. And to preserve the high conductivity of e-textiles, a 1 wt% (mass fractions) SBS/THF solution was prepared for encapsulating textile-AgNWs. As a result, the SEM images of e-textiles are presented in Fig. 1i and S4 (supporting information) where an ultrathin and homogeneous SBS layer is formed on the surface of hierarchical PU fibers.

The electronic conductivities of the textiles AgNWs and e-textiles on the number of dip-coating cycles are illustrated in Fig. 1j; within 8 dip-coating times, the conductivity of textile-AgNWs ascends from 0.21 S/m (1 dip-coating) to 8060 S/m (8 dip-coatings). And after SBS coating, the conductivity turns to, correspondingly, 0.11 S/m at first dip-coating and 7411 S/m at 8 cycles. Consequently, there is only a minute decrease in conductivity after the coating of SBS. However, the stability of the conductive network is significantly promoted due to the introduction of SBS. As shown in Fig. 1k, after continuous ultrasonic treatments in water bath (400 w), the electronic resistance of the textile-AgNWs increases exponentially at first 100 s; in contrast, the conductivity of e-textile remains essentially unchanged after 5000 s. Finally, the mechanical properties of fiber-shaped textile, textile-AgNWs, and e-textile are evaluated by tensile stress versus strain measurements (see Fig. 1l). The tensile stress at 140% strain is 0.39, 0.45, and 0.65 MPa, respectively, indicating that the SBS plays roles in both strengthening the structure mechanically and anchoring the AgNWs conductive network.
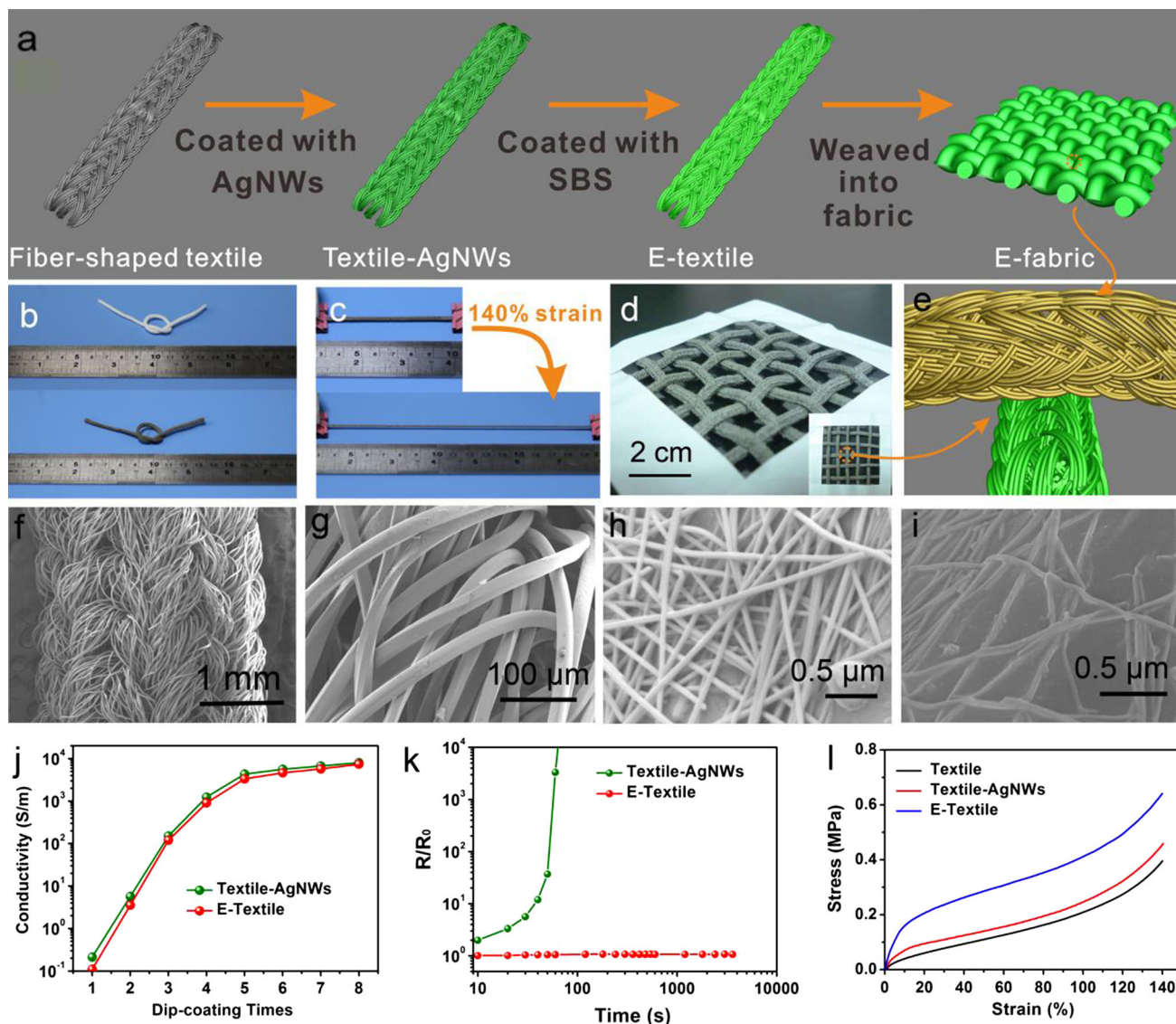
Figure 1 Fabrication of the e-textiles and e-fabric. **a** Schematic illustration of the fabrication processes of the e-textile and electronic fabric. **b** Optical images of the fiber-shaped textile before and after coating of AgNWs (8 dip-coating times) and SBS. **c** Digital photographs of the original and stretched e-textiles with a stretchability of 140%. **d** Digital photograph of the e-fabric. Inset is a top view of the e-fabric. **e** Schematic illustration of a sensor unit. **f, g** SEM images of fiber-shaped textile with different magnifications. **h** SEM image of the AgNWs coating on a hierarchical PU fiber (textile-AgNWs). **i** SEM image of the e-textile showing that AgNWs were fixed onto PU fiber by SBS. **j** Electrical conductivity change in the e-textiles before and after SBS coating at varying dip-coating times. **k** Resistance change (R/R_0) in the e-textiles before and after SBS coating as a function of ultrasonic time. **l** Stress versus strain curves of the fiber-shaped textile and the e-textiles before and after SBS coating.

To investigate the strain sensing performance of the e-textiles, a measure system consisting of a PC, a resistance analyzer, and a tensile machine with a step motor is installed (Fig. 2a, which can also be used for pressure sensing test). Next, the relative resistance changes (defined as R/R_0, where R and R_0 are the real-time and initial electronic resistance, respectively) in the e-textiles with different dip-coating

times under variable strains are measured and shown in Fig. 2b. It can be seen clearly that all the resistance changes increase after applied strain, but the resistance change slackens when dip-coating times increase. Typically, for 1 time dip-coating, the R/R_0 increases dramatically to 40 at 25% strain; however, the R/R_0 ascends gradually to 10 under 140% strain when dip-coating 8 times. The distinct difference can
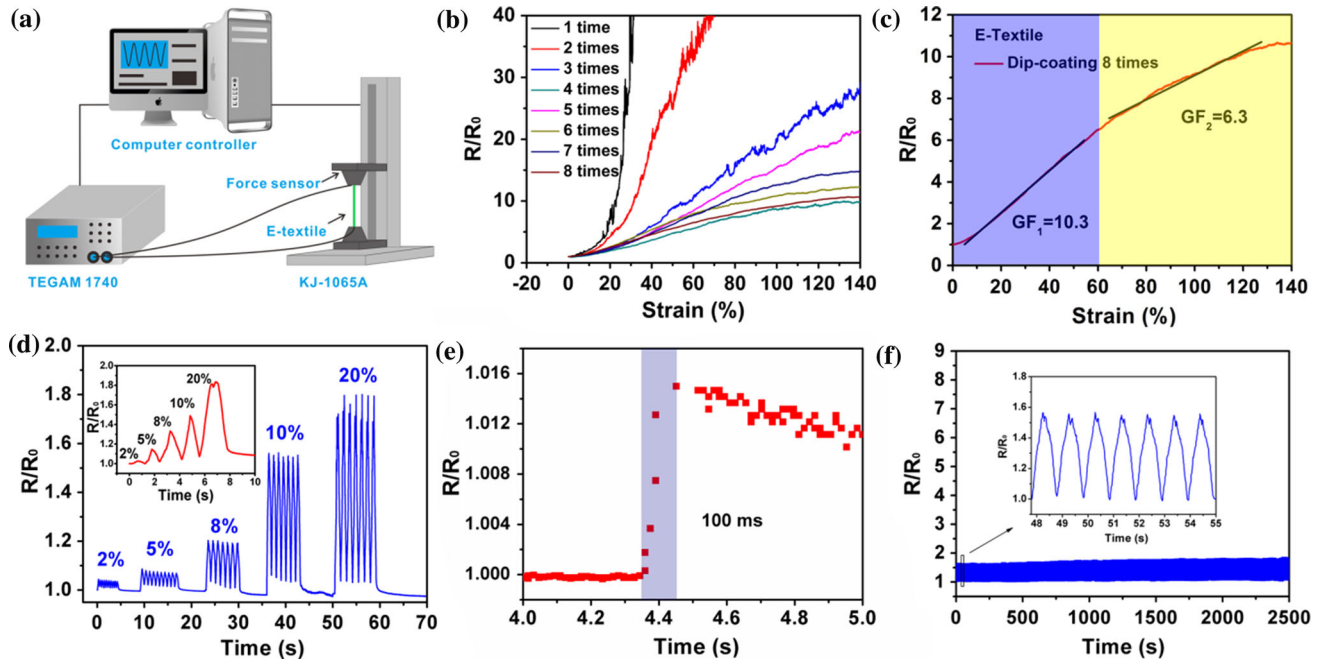
Figure 2 Strain sensing performance of the e-textiles. **a** Schematic illustration of the measurement setup. (The measurement setup can also be used for pressure sensing testing.) **b** Resistance change in e-textiles with different dip-coating times (1–8 times) relying on strain. **c** Change in resistance of e-textiles with 8 dip-coating times versus the applied strain; GF is calculated from the curve. **d** Resistance change in e-textiles (8 dip-coating times) under various applied cyclic strains (2, 5, 8, 10, and 20%, each strain is repeated 7 times). Inset is a gradually increasing step strain from 2 to 20%. **e** Response time measurement of e-textiles (1% strain applied, 500 mm/min) illustrates the response time is 100 ms. **f** Change in resistance for 2500 stretch-release cycles of strain variation from 0 to 10%, showing the stability of the sensor.

be explained by the structures of AgNWs networks: for 1 time dip-coating, AgNWs coated on the PU fibers are subtle and the gaps between adjacent fibers are partly disconnected (Fig. S3a, supporting information); thus, when strain is applied, the conductive network is easily broken resulting in a rapidly increasing in resistance and a greater noise fluctuations. Correspondingly, when the dip-coating cycles augment, AgNWs network becomes tighter and connects the gaps between neighboring PU fibers (Fig. S3e–h, supporting information). Therefore, the R/R_0 at 8 dip-coating times increases slowly when applied strain. This would also be ideally supported by the explanation "the conductive network is more stretchable when it is well above the percolation threshold" [38]. Considering of the original conductivity and conductive stability under tension, the e-textiles with 8 dip-coating times are chosen as our strain and pressure sensor. The gauge factor (GF, defined as $(R/R_0)/\varepsilon$) is employed to evaluate the tensile sensitivity; as illustrated in Fig. 2c, the resistance change has typical two stages relied on strain and in both stages the resistance changes have

excellent linearity (which is necessary for obtaining accurate output information) [39]. From the curve, the GF is calculated to be 10.3 under 60% strain and about 6.3 at strain 60–140%. Notably, the GF in the second stage (60–140% strain) is smaller than it in the first stage, differing from most reported traditional strain sensors. It can be attributed to the textile-based structure and the positive Possion's ratio (PPR) behavior of the strain sensor; the structure transformation (SEM images) and Possion's ratio as a function of strain are shown in Fig. S5 (supporting information); at first stage, the AgNWs network between neighboring hierarchical fibers was broken under strain, leading to a rapid increase in the resistance. At the second stage, because of the PPR behavior, a longitudinal tension brought about a radial compression (insets in Fig. S5, supporting information), which then results in a tardier increasing in resistance.

To further study the sensing capacity of the strain sensor, a gradually incremental step strain (2, 5, 8, 10, and 20%) is applied as illustrated in Fig. 2d inset; from the inset, the strain sensor has an accurate

response on various strain. What is more, the sensor has a superb mechanical stability since each strain is repeated 7 cycles as revealed in Fig. 2d. The response time to strain (1% strain, 500 mm/min) is given in Fig. 2e; the fast response (100 ms) based on textile-based structure undoubtedly promotes the real-time monitoring of fast and intricate motions. Additionally, about 2500 cycles (10% strain) are performed and the corresponding resistance changes are real-time recorded (Fig. 2f). The excellent stability allows the sensors a reliable practical application as daily strain sensors. Table S1 (supporting information) displays the main strain performance of fiber-shaped strain sensors reported before as comparison.

Significantly, the e-textiles can be used in pressure sensing field for capturing microstrain and tactile touching, which are necessary for full-range detection of human motions. Figure 3a illustrates the resistance change under various pressure. (Schematic is displayed in Fig. 3a inset.) The resistance change decreases when applied pressure and the pressure sensitivity (S, defined as $S = \Delta(R/R_0)/\Delta P$) were calculated by the slope of the curve; it can be seen that the sensitivities under low loading force are 0.20 and 0.009 kPa^{-1} under high loading force range. The sensitivity is higher than most previously reported fiber-shaped pressure sensors as listed in Table S1 (supporting information). Moreover, the cycle testing is taken under a step pressure as presented in Fig. 3b; each pressure is cycled 6 times and the result shows the pressure sensor is high-resolution, reproducible, and stable.

The high pressure sensitivity resulted mainly from the inherent hierarchical structure of the e-textile. It is generally accepted that the dominant sensing mechanisms of piezoresistive sensors under pressure contain two parts: (1) increasing the contact area and (2) increasing the contact paths [29, 34, 39]. Herein, the high sensitivity can be perfectly explained by the two mechanisms. For the first mechanism, when applied pressure, the continuous AgNWs networks located in the neighboring PU fibers (Fig. S3h, supporting information) will be compressed, resulting in an increase in contact area. For the second mechanism, as shown in Fig. 1f, g, the fiber-shaped textile is knitted by hierarchical microscale PU fibers, and distance exists between further fibers (Fig. 3c, d, and S6a, supporting information). Before loading force, the total resistance of the e-textiles (R_{total}) is

determined by contact resistance (R_c) and bulk resistance (R_{bulk}) and expressed by:

$$R_{total} = R_{bulk} + R_c \tag{1}$$

The corresponding circuit diagram is presented in Fig. 3c inset. In this condition, since the R_{bulk} is not directly contact with the electrodes, R_{total} is dominated by R_c due to the separated morphology. After force loaded, the space between fibers is reduced, resulted in the fast increase in contact paths as illustrated in Fig. 3e, f, and S6b (supporting information). With this structure, the circuit diagram is given in Fig. 3e and the R_{total} can be expressed as follows:

$$\begin{aligned} R_{total} &= R_{bulk} + R_c \\ &= R_{bulk} + \frac{1}{1/R_{c_1} + 1/R_{c_2} + 1/R_{c_3} + \cdots + 1/R_{c_n}} \end{aligned} \tag{2}$$

We can see in Eq. (2) that the R_c decreased rapidly with the increase in conductive paths. The two mechanisms jointly lead to the high sensitivity of the pressure sensor.

Additionally, owing to the textile-based structure the e-textiles also exhibit fast response to force (10 kPa was applied instantaneously). As shown in Fig. 3g, the response time and relaxation time are 13 and 53 ms, respectively. Figure 3h reveals that the pressure sensor also has a low detection limit (20 mg) and can be applied to feel subtle forces. Finally, the compression stability is further researched by loaded/unloaded periodic pressure (10 kPa, ~ 1 Hz) on the e-textiles and the resistance variation is real time shown in Fig. 3i; it can be seen that the resistance almost keeps unchanged even after more than 6000 cycles, indicating the superb stability and reproducibility of the e-textile as pressure sensor.

Owing to the excellent strain sensing (high stretchability and high gauge factor) and pressure sensing (high sensitivity and fast responsibility) performance, the e-textile processes tremendous potential applications as wearable electronics for full-range detection of human motions. For vigorous motion sensing, an e-textile was fixed onto a finger for racing of finger bending; as shown in Fig. 4a, different bending angles (30° and 90°, as defined in inset) could be precisely tracked by real-time monitoring the change in resistance. In pressure singles (or subtle human motions) detection, the e-textile could be used to detect phonation. Typically, the e-textile was attached onto throat for signals capturing (Fig. 4b). In Fig. 4b, when the human spoke four
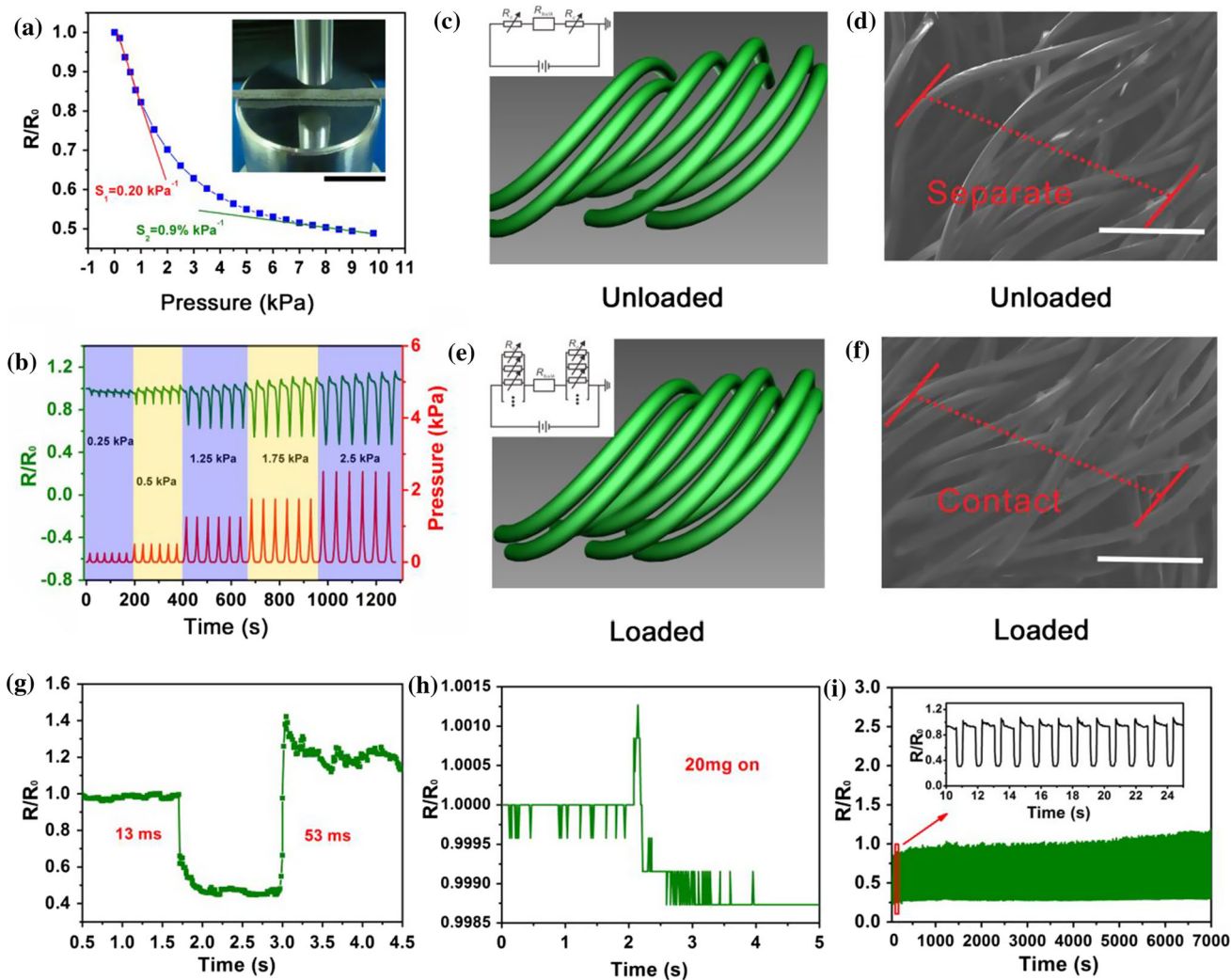
Figure 3 Pressure sensing properties of the e-textiles. **a** Resistance change under various pressures. Inset is the optical image of e-textiles under pressure, scale bar: 2 cm. **b** Normalized resistance changes varying the applied pressure at 0.25, 0.5, 1.25, 1.75, and 2.5 kPa. Each pressure is repeated 6 times. **c**–**f** Schematic illustrations and SEM images of textiles structural changes before (**c**, **e**) and after (**d**, **f**) force loaded, scale bar: 100 μm. Insets are equivalent circuit diagrams of these two structures. **g** Response time measurement reveals a 13 ms of response time and 53 ms of relax time. **h** Resistance change after 20 mg weight on the sensor. **i** Total resistance and waveforms of the pressure sensor show superb working stability even after more than 6000 loading/unloading cycles.

letters named "S," "C," "U," and "T," the response curves exhibited typical different peaks with good repeatability, indicating the sensor's excellent capability of distinguishing phonation, with potential applications in human/machine interaction and phonation rehabilitation.

For health monitoring, pulse is a key physiological signal for determining the systolic and diastolic blood pressure and the heart rate. Figure 4c presents the record of 12 pulse periods in 7 s, indicating the heartbeat of 102 times per minute. What is more, the enlarge view of a single pulse peak clearly reveals a

typical characteristic pulse waveform with three easily recognizable peaks, named percussion wave, tidal wave, and diastolic wave (Fig. 4d), demonstrating the sensor's fast responsibility and promising using for disease diagnosis. Moreover, an e-textile was then attached onto a human's nape for monitoring of neck motions; as presented in Fig. 4e–l, the e-textile could accurately discriminate different neck activities (down, up, left, and right) by means of the obviously differentiated patterns of response curves, indicating its great potentials in scoliosis correcting. In daily life, restless legs syndrome (RLS) is a typical
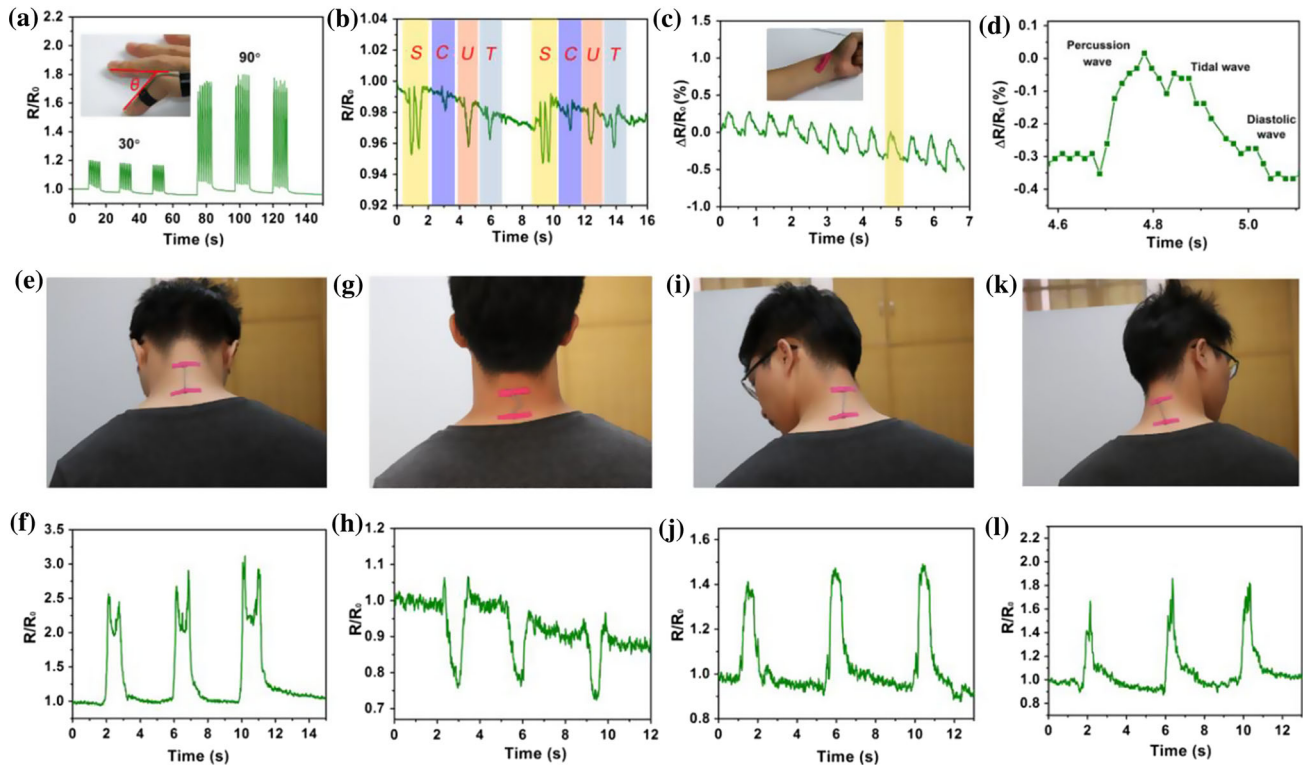
Figure 4 Applications of the e-textiles. **a** Change in resistance of the wearable sensor in monitoring of finger bending. Inset is the optical image of wearable sensor integrating on a finger. **b** Responsive curves real-time recorded during the speaking of "S," "C," "U," and "T," respectively. **c** Resistance change as a function of time for measurement of pulse beating. Inset is the digital photograph to show the wearable sensor is attached on the wrist. **d** Enlarge view of the orange area in (**c**). (**e**–**l**) Digital photographs show that an e-textile was attached on a human's nape and corresponding resistance changes when the human's neck turns down (**e**, **f**), up (**g**, **h**), left (**i**, **j**), and right (**k**, **l**).

neurological sensory-motor disorder with symptoms of restless and unpleasant shaking or moving legs even during periods of rest or inactivity [40]. Thus, the real-time monitoring of leg vibration would benefit the early diagnosing of RLS. In this case, an e-textile was integrated on a human's knee for RLS simulation; as it can be seen in Fig. S7 (supporting information), the high-frequency (6 HZ) leg shaking could be easily and successfully reflected by the fast and stable change in resistance, indicating the e-textile's excellent potentials in RLS diagnosing.

Weavability is another prominent advantage of fiber-shaped wearable sensors compared to traditional planar and cubic sensors. By woven into fabrics, it can precisely detect the position and distribution of mechanical stimuli. In this research, we fabricated a proof-of-concept e-fabric with 10×10 pixels sensing arrays; the photograph and schematic model are provided in Fig. 5e, f, respectively. To study the working mechanism of the as-

prepared electronic fabric, a sensor unit was developed by stacking two e-textiles perpendicular to each other (inset in Fig. 5a), and the piezoresistive behavior of sensor unit was further researched. Figure 5a shows the resistance change in the sensor unit as a function of applied pressure. And the sensitivity of the sensor unit is then calculated from the slop of the curve. It can be seen that the sensitivity (1.03 kPa^{-1}) at low loading force (0.2 kPa) is much higher than it (0.28 kPa^{-1}) at high loading force (0.2–2 kPa). To further study the sensing capacity of the sensor unit under micropressure, a gradually increasing step pressure test was processed; as illustrated in Fig. 5b, the sensor unit has precise responses to different pressures (0.05, 0.07, 0.09, 0.11, and 0.13 kPa) and the response is stable, reproducible since every force is loaded five times. The superb high sensitivity under low pressure can be attributed to the change in contact resistance at the cross-contact point between two e-textiles. As revealed in Fig. 5c, the edge of the
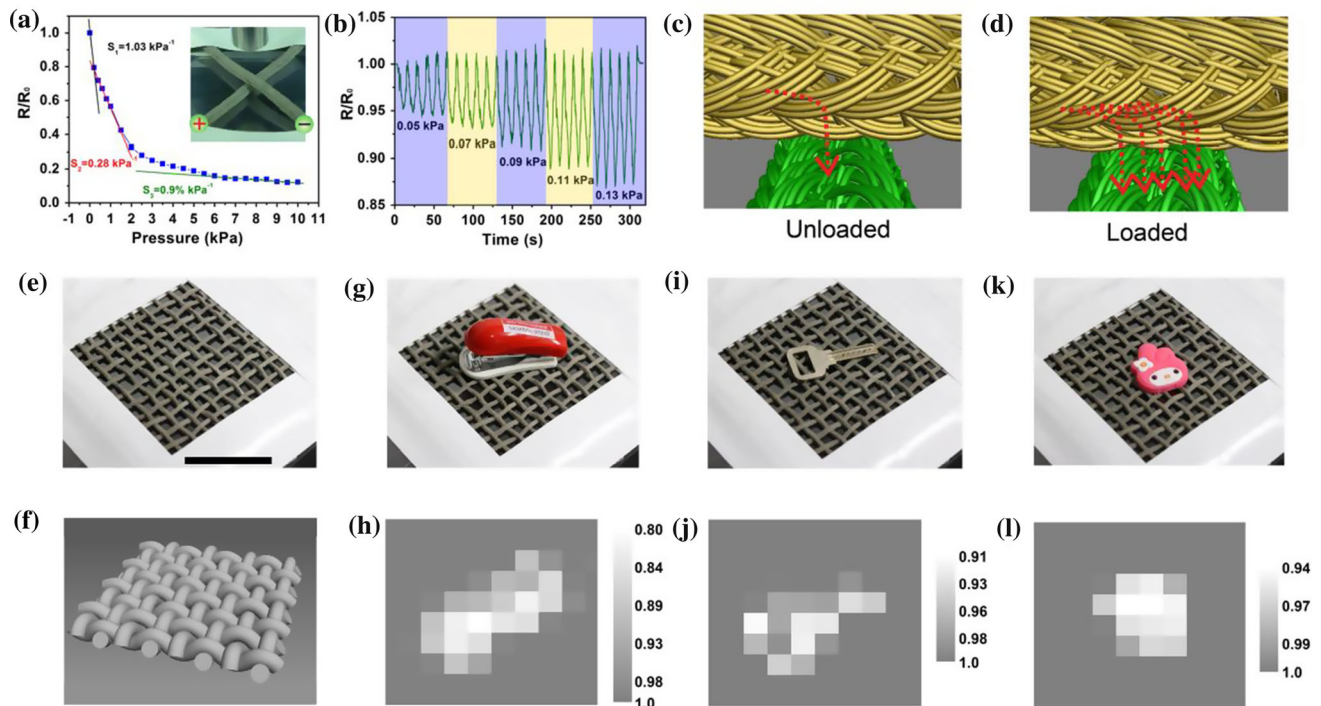
Figure 5 Pressure sensing properties of the sensor unit and force mapping properties of the e-fabric. **a** Resistance change under various pressures. Inset is the optical image of the sensor unit under pressure. **b** Resistance changes under gradually increasing micropressure at 0.05, 0.07, 0.09, 0.11, and 0.13 kPa. Each pressure is repeated 5 times. **c**, **d** Schematic illustrations of the sensor unit structural changes before (**c**) and after (**d**) force loaded. **e**, **f** Optical image and schematic illustration of the as-prepared electronic fabric, scale bar: 5 cm. **g**–**l** Digital photographs of the electronic fabric with a mini stapler (**g**), a key (**i**), and a rubber pendant (**k**) loaded and the reflected 2D intensity mapping of resistance changes for each sensor unit (**h**, **j**, and **l**).

e-textile is composed of plenty of microscale PU fibers with a wave-like morphology, to the best of our knowledge, the wave-like morphology is very helpful for developing sensitive piezoresistive sensors [22]; after loading a subtle pressure, both the contact paths and contact area between the two e-textiles increased as presented in Fig. 5d, resulting in the rapid fall in resistance.

To demonstrate the force mapping ability of the as-prepared e-fabric (Fig. 5e, f), different shape and weight daily supplies were placed onto the e-fabric, and the resistance change between each row and vertical was measured before and after the loading. To exhibit the 2D forcing map clearly on the fabric by recording the resistance change, each sensor unit was noted as defined in Fig. S8 (supporting information). Figure 5g, i, and k shows that a mini stapler (25.3 g), a key (9.3 g), and a rubber pendant (3.5 g) were loaded on the fabric, and the resistance changes are gathered and plotted into 2D maps as performed in Fig. 5h, j, and l, respectively. The results show that both the material shapes and weights can be clearly distinguished by the color contrast mapping. Finally, the electronic fabric has great potentials in artificial skin and smart fabric because it can provide a spatial distribution map that reflected the touch positions and pressure.

Conclusion

In summary, we herein develop a fiber-shaped e-textile using PU fibers, AgNWs, and SBS via knitting and simple dip-coating processes. The e-textile has a high initial conductivity of 7.4×10^3 S/m and a high stretchability (140%). Due to the textile-based structures and hierarchical fibers, the e-textile exhibits good capability of detecting multiple deformation including tensile strain and pressure, which enables their full-range detection of human motions. The high stretchability, high sensitivity, and fast responses also make the e-textiles further applied in health monitoring such as pulse beating detection, scoliosis correcting, and PLS diagnosing. Moreover,

the e-textile's fibrous architecture endows the e-textiles being woven into e-fabric, and the sensing mechanism is further researched, after that we demonstrate the e-fabric can be successfully used to map force distribution and pressure. Therefore, with the fiber-shaped characters, textile-based structures, and hierarchical fiber layout, the e-textiles show huge potentials in diverse wearable and smart devices in the future.

Acknowledgements

Electronic supplementary material: The online version of this article (doi:10.1007/s10853-017-1644-y) contains supplementary material, which is available to authorized users.

References

[1] Jin H, Matsuhisa N, Lee S et al (2017) Enhancing the performance of stretchable conductors for e-textiles by controlled ink permeation. Adv Mater 29:1605848

[2] Zhang M, Wang C, Wang H et al (2017) Carbonized cotton fabric for high-performance wearable strain sensors. Adv Funct Mater 27:1604795

[3] Cai G, Yang M, Xu Z et al (2017) Flexible and wearable strain sensing fabrics. Chem Eng J 325:396–403

[4] Lee T, Lee W, Kim S-W et al (2016) Flexible textile strain wireless sensor functionalized with hybrid carbon nanomaterials supported ZnO nanowires with controlled aspect ratio. Adv Funct Mater 26:6206–6214

[5] Zhao Z, Yan C, Liu Z et al (2016) Machine-washable textile triboelectric nanogenerators for effective human respiratory monitoring through loom weaving of metallic yarns. Adv Mater 28:10267–10274

[6] Zhou G, Byun J-H, Oh Y et al (2017) Highly sensitive wearable textile-based humidity sensor made of high-strength, single-walled carbon nanotube/poly(vinyl alcohol) filaments. ACS Appl Mater Interfaces 9:4788–4797

[7] Wang C, Zhang M, Xia K et al (2017) Intrinsically stretchable and conductive textile by a scalable process for elastic wearable electronics. ACS Appl Mater Interfaces 9:13331–13338

[8] Fu Y, He H, Liu Y et al (2017) Self-powered, stretchable, fiber-based electronic-skin for actively detecting human motion and environmental atmosphere based on a triboelectrification/gas-sensing coupling effect. J Mater Chem C 5:1231–1239

[9] Lou Z, Chen S, Wang L et al (2016) An ultra-sensitive and rapid response speed graphene pressure sensors for electronic skin and health monitoring. Nano Energy 23:7–14

[10] Liu S, Hu M, Yang J (2016) A facile way of fabricating a flexible and conductive cotton fabric. J Mater Chem C 4:1320–1325

[11] Wei Y, Chen S, Dong X et al (2017) Flexible piezoresistive sensors based on "dynamic bridging effect" of silver nanowires toward graphene. Carbon 113:395–403

[12] Wei Y, Chen S, Lin Y et al (2016) Silver nanowires coated on cotton for flexible pressure sensors. J Mater Chem C 4:935–943

[13] Eom J, Jaisutti R, Lee H et al (2017) Highly sensitive textile strain sensors and wireless user-interface devices using all-polymeric conducting fibers. ACS Appl Mater Interfaces 9:10190–10197

[14] Seyedin S, Razal JM, Innis PC et al (2015) Knitted strain sensor textiles of highly conductive all-polymeric fibers. ACS Appl Mater Interfaces 7:21150–21158

[15] Wang C, Li X, Gao E et al (2016) Carbonized silk fabric for ultrastretchable, highly sensitive, and wearable strain sensors. Adv Mater 28:6640–6648

[16] Park J, Lee Y, Hong J et al (2014) Tactile-Direction-sensitive and stretchable electronic skins based on human-skin-inspired interlocked microstructures. ACS Nano 8:12020–12029

[17] Frutiger A, Muth JT, Vogt DM et al (2015) Capacitive soft strain sensors via multicore-shell fiber printing. Adv Mater 27:2440–2446

[18] Lee J, Kwon H, Seo J et al (2015) Conductive fiber-based ultrasensitive textile pressure sensor for wearable electronics. Adv Mater 27:2433–2439

[19] Cooper CB, Arutselvan K, Liu Y et al (2017) Stretchable capacitive sensors of torsion, strain, and touch using double helix liquid metal fibers. Adv Funct Mater 27:1605630

[20] Wang H, Liu Z, Ding J et al (2016) Downsized sheath-core conducting fibers for weavable superelastic wires,

biosensors, supercapacitors, and strain sensors. Adv Mater 28:4998–5007

[21] Lee S, Shin S, Lee S et al (2015) Ag nanowire reinforced highly stretchable conductive fibers for wearable electronics. Adv Funct Mater 25:3114–3121

[22] Wei Y, Chen S, Yuan X et al (2016) Multiscale wrinkled microstructures for piezoresistive fibers. Adv Funct Mater 26:5078–5085

[23] He X, Zi Y, Guo H et al (2017) A highly stretchable fiber-based triboelectric nanogenerator for self-powered wearable electronics. Adv Funct Mater 27:1604378

[24] Zhao Z, Yan C, Liu Z et al (2016) Machine-washable textile triboelectric nanogenerators for effective human respiratory monitoring through loom weaving of metallic yarns. Adv Mater 28:10267–10274

[25] Cheng Y, Wang R, Sun J, Gao L (2015) A stretchable and highly sensitive graphene-based fiber for sensing tensile strain, bending, and torsion. Adv Mater 27:7365–7371

[26] Liu ZF, Fang S, Moura FA et al (2015) Hierarchically buckled sheath-core fibers for superelastic electronics, sensors, and muscles. Science 349:400–404

[27] Foroughi J, Spinks GM, Aziz S et al (2016) Knitted carbon-nanotube-sheath/spandex-core elastomeric yarns for artificial muscles and strain sensing. ACS Nano 10:9129–9135

[28] Cheng Y, Wang R, Sun J, Gao L (2015) Highly conductive and ultrastretchable electric circuits from covered yarns and silver nanowires. ACS Nano 9:3887–3895

[29] Park J, Lee Y, Hong J et al (2014) Giant tunneling piezoresistance of composite elastomers with interlocked microdome arrays for ultrasensitive and multimodal electronic skins. ACS Nano 8:4689–4697

[30] Zhong W, Liu Q, Wu Y et al (2016) A nanofiber based artificial electronic skin with high pressure sensitivity and 3D conformability. Nanoscale 8:12105–12112

[31] Wang X, Gu Y, Xiong Z et al (2014) Silk-molded flexible, ultrasensitive, and highly stable electronic skin for monitoring human physiological signals. Adv Mater 26:1336–1342

[32] Jian M, Xia K, Wang Q et al (2017) Flexible and highly sensitive pressure sensors based on bionic hierarchical structures. Adv Funct Mater 27:1606066

[33] Wang Z, Wang S, Zeng J et al (2016) High sensitivity, wearable, piezoresistive pressure sensors based on irregular microhump structures and its applications in body motion sensing. Small 12:3827–3836

[34] Tai Y, Lubineau G (2016) Double-twisted conductive smart threads comprising a homogeneously and a gradient-coated thread for multidimensional flexible pressure-sensing devices. Adv Funct Mater 26:4078–4084

[35] Ge J, Sun L, Zhang F-R et al (2016) A stretchable electronic fabric artificial skin with pressure-, lateral strain-, and flexion-sensitive properties. Adv Mater 28:722–728

[36] Sun Q, Seung W, Kim BJ et al (2015) Active matrix electronic skin strain sensor based on piezopotential-powered graphene transistors. Adv Mater 27:3411–3417

[37] Chen S, Wei Y, Wei S et al (2016) Ultrasensitive cracking-assisted strain sensors based on silver nanowires/graphene hybrid particles. ACS Appl Mater Interfaces 8:25563–25570

[38] Kim KK, Hong S, Cho HM et al (2015) Highly sensitive and stretchable multidimensional strain sensor with prestrained anisotropic metal nanowire percolation networks. Nano Lett 15:5240–5247

[39] Bae GY, Pak SW, Kim D et al (2016) Linearly and highly pressure-sensitive electronic skin based on a bioinspired hierarchical structural array. Adv Mater 28:5300–5306

[40] Ekbom K, Ulfberg J (2009) Restless legs syndrome. J Intern Med 266:419–431